Spectrally-invariant approximation within atmospheric radiative transfer

A. Marshak

Climate and Radiation Branch, NASA Goddard Space Flight Center, Greenbelt, Maryland

Y. Knyazikhin

Department of Geography and Environment, Boston University, Boston, Massachusetts

J. C. Chiu

Department of Meteorology, University of Reading, Reading, UK

W. J. Wiscombe

Climate and Radiation Branch, NASA Goddard Space Flight Center, Greenbelt, Maryland

Submitted for publication in

JOURNAL OF THE ATMOSPHERIC SCIENCE

Submitted: May 27, 2011

Corresponding Author: Alexander Marshak

email: Alexander.Marshak@nasa.gov

Spectrally Invariant Approximation within Atmospheric Radiative Transfer

A. MARSHAK

Climate and Radiation Branch, NASA Goddard Space Flight Center, Greenbelt, Maryland

Y. KNYAZIKHIN

Department of Geography and Environment, Boston University, Boston, Massachusetts

J. C. CHIU

Department of Meteorology, University of Reading, Reading, United Kingdom

W. J. WISCOMBE

Climate and Radiation Branch, NASA Goddard Space Flight Center, Greenbelt, Maryland

(Manuscript received 14 February 2011, in final form 25 May 2011)

ABSTRACT

Certain algebraic combinations of single scattering albedo and solar radiation reflected from, or transmitted through, vegetation canopies do not vary with wavelength. These "spectrally invariant relationships" are the consequence of wavelength independence of the extinction coefficient and scattering phase function in vegetation. In general, this wavelength independence does not hold in the atmosphere, but in cloud-dominated atmospheres the total extinction and total scattering phase function vary only weakly with wavelength. This paper identifies the atmospheric conditions under which the spectrally invariant approximation can accurately describe the extinction and scattering properties of cloudy atmospheres. The validity of the assumptions and the accuracy of the approximation are tested with 1D radiative transfer calculations using publicly available radiative transfer models: Discrete Ordinate Radiative Transfer (DISORT) and Santa Barbara DISORT Atmospheric Radiative Transfer (SBDART). It is shown for cloudy atmospheres with cloud optical depth above 3, and for spectral intervals that exclude strong water vapor absorption, that the spectrally invariant relationships found in vegetation canopy radiative transfer are valid to better than 5%. The physics behind this phenomenon, its mathematical basis, and possible applications to remote sensing and climate are discussed.

1. Introduction

Recently several papers reported the discovery of spectrally invariant behavior in some simple algebraic combinations, called "spectral invariants," of single scattering albedo and solar radiation reflected from or transmitted through vegetation canopies (Knyazikhin et al. 1998, 2005; Huang et al. 2007). The spectral invariant phenomenon is clearly seen in radiative measurements and remote sensing data (Panferov et al. 2001; Wang et al. 2003). The phenomenon was theoretically explained and numerically simulated using radiative transfer theory (Knyazikhin et al. 2011; Smolander and Stenberg 2005). There are three key parameters that characterize the radiative transfer process: the extinction coefficient, scattering phase function, and single scattering albedo. In vegetation, the optical distance between two points within the canopy does not depend on wavelength because the scattering elements are much larger than the wavelength of solar radiation (Ross 1981). And the canopy scattering phase function is also wavelength independent since it is determined by large scattering elements such as twigs and leaves. Thus, of the three key variables, the single scattering albedo is the only one with significant wavelength dependency. This allows for a natural separation between structural and spectral parameters of radiative transfer: the extinction coefficient

Corresponding author address: Alexander Marshak, Climate and Radiation Branch, NASA Goddard Space Flight Center, Greenbelt, MD 20771.
E-mail: alexander.marshak@nasa.gov

DOI: 10.1175/JAS-D-11-060.1

and scattering phase function are purely structural, while the single scattering albedo is purely spectral.

This separation does not hold for the atmosphere where extinction and scattering due to Rayleigh molecules and aerosols, as well as gaseous absorption, depend strongly on wavelength. However, under some cloudy atmospheric conditions the physical processes that vary weakly with wavelength (e.g., cloud scattering) may dominate. Then, for a large range of wavelengths, the extinction coefficient and the scattering phase function may be weakly spectrally variable.

In loose analogy with the structural/spectral separation that occurs in vegetation radiative transfer, the standard method for cloud remote sensing from space (Nakajima and King 1990) retrieves optical depth and droplet effective radius. Optical depth is the structural parameter with no significant wavelength dependence, while effective radius strongly affects single scattering albedo (Twomey and Bohren 1980). The Nakajima–King method decomposes the radiative measurements into structural (optical depth) and spectral (effective radius) parameters. It takes advantage of the fact that radiation in the visible, where particles do not absorb, is much more sensitive to cloud optical depth than to droplet size. In contrast, in the near infrared, where water absorbs, the radiance changes substantially with effective radius and is insensitive to cloud optical depth, at least for thicker clouds.

The above analogy between cloud and vegetation remote sensing is not perfect because generally cloud droplet size also affects the scattering phase function. However, we can still ask how well the spectral invariant approach in vegetation canopies works for cloudy atmospheres. The goal of this paper is to answer that question.

The plan of the paper is as follows. In the next section we sketch the general concept of spectral invariance (SI) and demonstrate its validity with simple Discrete Ordinate Radiative Transfer model (DISORT) calculations. Section 3 looks at the extent to which the spectral variability of the extinction and scattering properties in cloudy atmospheres meets the needs of spectral invariance theory. Section 4 illustrates the spectrally invariant behavior of radiances and fluxes and discusses its physical interpretation. Accuracy of the spectral invariant approximation is discussed in section 5, and section 6 briefly describes its possible implementations in remote sensing and climate modeling. Finally, the appendix provides a physical and mathematical basis for spectral invariance.

2. Spectral invariance

Spectral invariance states that simple algebraic combinations of the spectra of single scattering albedo and

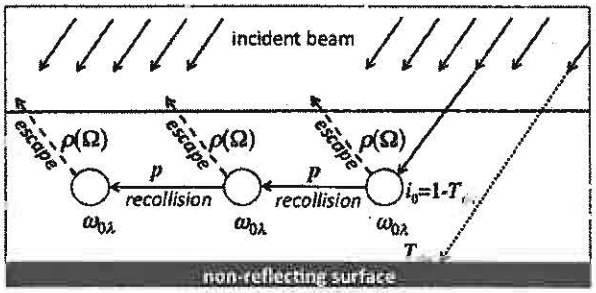

FIG. 1. Schematic of radiative transfer process. The term T_{dir} is the fraction of photons in the incident beam that reach the surface without interacting. A fraction $i_0 = 1 - T_{\text{dir}}$ therefore interacts with the medium. With probability $\omega_{0\lambda}$, these photons are scattered and then either interact again (with probability p) or escape the medium in direction Ω [with probability $\rho(\Omega)$].

reflected and/or transmitted radiation eliminate the dependences on wavelength (Huang et al. 2007; Knyazikhin et al. 2011). In many cases spectral dependency can be compressed into a linear relationship

$$y(\lambda) = ax(\lambda) + b, \tag{1}$$

where parameters a and b are independent of wavelength λ, and functions $y(\lambda)$ and $x(\lambda)$ are algebraic combinations of measured spectra.

Spectrally invariant relationships were originally derived for vegetation canopies with "black" soil. Here we briefly summarize the "nontraditional" derivation (e.g., Schull et al. 2007) of radiative transfer in an absorbing and reflecting layer, following the diagram in Fig. 1. We should emphasize that we assume that the standard diffuse–direct transformation of the radiative transfer equation has been applied; we are only dealing with the diffuse part.

Let T_{dir} be the direct transmittance—that is, the fraction of photons from the incident beam that pass through the layer in Fig. 1 without colliding. With probability ω_0 a collided photon will be scattered and will either recollide or escape the layer in a given direction Ω with probabilities p and $\rho(\Omega)$, respectively. Here ω_0, p, and $\rho(\Omega)$ are the single scattering albedo, recollision probability, and directional escape probability, respectively.

While ω_0 is a well-known parameter in atmospheric radiation, p and $\rho(\Omega)$ are less known and thus require some explanation: p is the conditional probability that a scattered photon will interact with the medium again (Smolander and Stenberg 2005), and $\rho(\Omega)$ is the conditional probability that a scattered photon will leave the medium in the direction Ω. The parameters p and ρ are simply related. Let us assume for simplicity that $T_{\text{dir}} = 0$. If p is the probability of recollision, then $1 - p$ is the total escape probability and (e.g., Schull et al. 2011)

$$\int_{4\pi} \rho(\Omega)|\mu|\, d\Omega = 1 - p, \tag{2}$$

where μ is the cosine of a polar angle of Ω. Here $\rho(\Omega)/(1-p)$ is the probability density of escape in Ω as a result of one interaction; it can be considered as the whole domain counterpart of the scattering phase function. In general, p and ρ depend on the successive order of scattering; however, this dependence weakens as the number of interactions increases (Huang et al. 2007).

If we assume that p and ρ do not depend on the scattering order, the probability that a photon will escape the layer after m interactions is $i_0 \rho p^{m-1} \omega_{0\lambda}^m$, where $i_0 = 1 - T_{\text{dir}}$ is the fraction of incoming photons that collide within the layer (Fig. 1). For a purely absorbing surface (zero lower boundary condition), the fraction of exiting photons in a given Ω is simply the sum of these probabilities over scattering order m; that is,

$$\begin{aligned} I_\lambda(\Omega) &= \rho(\Omega)\omega_{0\lambda} i_0 + \rho(\Omega)\omega_{0\lambda}^2 p i_0 + \cdots \\ &\quad + \rho(\Omega)\omega_{0\lambda}^m p^{m-1} i_0 + \cdots \\ &= \frac{\omega_{0\lambda}}{1 - p\omega_{0\lambda}} \rho(\Omega) i_0. \end{aligned} \tag{3}$$

So far we have suppressed wavelength dependency in all quantities except I and ω_0; ω_0 is assumed to be the only spectrally varying parameter. Equation (3) can be rearranged as

$$\frac{I_\lambda(\Omega)}{\omega_{0\lambda}} = p I_\lambda(\Omega) + \rho(\Omega) i_0. \tag{4}$$

If p and ρi_0 do not depend on wavelength, Eq. (4) qualifies as an SI relationship [Eq. (1)].

Under what conditions is Eq. (4) valid in the atmosphere? In vegetation canopies the extinction coefficient σ is wavelength independent—that is,

$$\sigma(\lambda) \equiv \sigma \tag{5a}$$

—and the scattering phase function P does not depend on wavelength either:

$$P(\Omega, \Omega', \lambda) = P(\Omega, \Omega'). \tag{5b}$$

The single scattering albedo $\omega_{0\lambda}$ thus becomes the only spectrally varying parameter in the radiative transfer equation. As a result, p and $\rho(\Omega)$ become wavelength independent (Knyazikhin et al. 2011). In this case, Eq. (4) forms a straight line on the $I_\lambda/\omega_{0\lambda}$ versus I_λ plane where slope and intercept give p and escape factor ρi_0. (A formal definition of the recollision probability in terms of the 3D radiative transfer equation is given in the appendix).

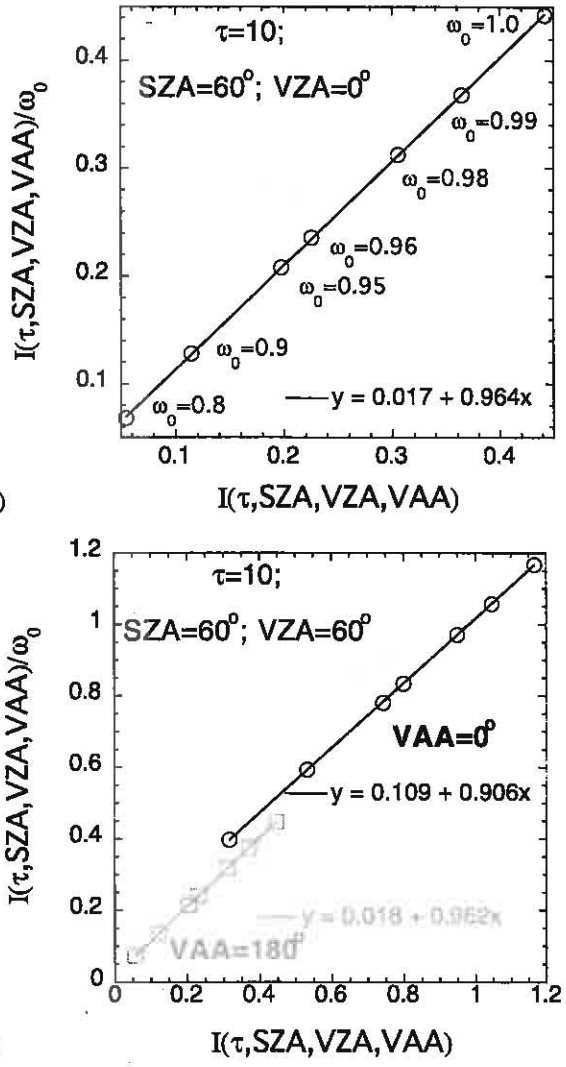

FIG. 2. Linear relationship between the ratio I/ω_0 and I (I is reflected radiance) for $\tau = 10$, and for seven values of ω_0 from 0.8 to 1.0. A Henyey–Greenstein scattering phase function with asymmetry factor $g = 0.85$ is used. The surface is black. The 1D radiative transfer code DISORT is used to calculate values of $I(\tau$, SZA, VZA, VAA) where SZA, VZA, and VAA are the solar zenith, viewing zenith, and viewing azimuth angles, respectively. SZA is 60°. (a) VZA = 0°. (b) VZA = 60°; VAA = 0° (black circles) and VAA = 180° (gray squares).

Figure 2 illustrates the validity of Eq. (4) using the 1D radiative transfer code DISORT (Stamnes et al. 1988) with the Henyey–Greenstein scattering phase function for a cloud with optical depth $\tau = 10$ and different values of ω_0 between 0.8 and 1. Although the slope a (an approximation of p) is mostly determined by the medium internal structure given by σ and P (Smolander and Stenberg 2005), it also depends weakly on the solar-viewing geometry as shown in Fig. 2b. However, the

viewing geometry mostly affects the intercept of the linear relationship b, an approximation of $\rho(\Omega)$.

Obviously, the assumptions in Eqs. (5a) and (5b) are not met for the atmosphere where both the extinction due to molecular and aerosol scattering and the gaseous absorption strongly depend on wavelength. However, for cloudy conditions and certain wavelength ranges, the physical processes that vary only weakly with λ may dominate. As a result, the atmospheric extinction coefficient and the scattering phase function may be approximately constant there. Section 3 explores this possibility.

3. Spectral variability of the extinction and scattering properties in real atmosphere

Let us calculate the total extinction coefficient as a function of wavelength:

$$\sigma_\lambda = \sum_{k=1}^{N} \sigma_{k,\lambda} = \sum_{k=1}^{N} (\sigma_{sk,\lambda} + \sigma_{ak,\lambda}) = \sigma_{s,\lambda} + \sigma_{a,\lambda}. \tag{6a}$$

Here index k refers to the kth atmospheric constituent, s to scattering, and a to absorption; for example, Rayleigh molecules ($\sigma_{s,\lambda} \neq 0, \sigma_{a\lambda} = 0$), aerosol particles ($\sigma_{s,\lambda} \neq 0$, $\sigma_{a\lambda} \neq 0$), cloud droplets ($\sigma_{s,\lambda} \neq 0, \sigma_{a,\lambda} \neq 0$), and gaseous absorbers ($\sigma_{s\lambda} = 0, \sigma_{a,\lambda} \neq 0$). In the radiative transfer equation the total (or effective) single scattering albedo is defined as

$$\omega_{0\lambda} = \frac{1}{\sigma_\lambda} \sum_{k=1}^{N} \sigma_{k\lambda} \omega_{0k,\lambda} = \frac{1}{\sigma_\lambda} \sum_{k=1}^{N} \sigma_{sk,\lambda} = \frac{\sigma_{s,\lambda}}{\sigma_\lambda}. \tag{6b}$$

For simplicity, we will characterize the scattering phase function with the asymmetry parameter:

$$g_\lambda = \frac{1}{\sigma_{s,\lambda}} \sum_{k=1}^{N} \sigma_{sk,\lambda} g_{k,\lambda}. \tag{6c}$$

Instead of the total extinction coefficient we will use the total optical depth:

$$\tau_\lambda = \sum_{k=1}^{N} \tau_{k,\lambda} = \sum_{k=1}^{N} (\tau_{sk,\lambda} + \tau_{ak,\lambda}) = \tau_{s,\lambda} + \tau_{a,\lambda}. \tag{6d}$$

For three values of cloud optical depth, Fig. 3 illustrates the total optical depth $\tau_\lambda = \tau_{R\lambda} + \tau_{A\lambda} + \tau_{C\lambda} + \tau_{G\lambda}$ and each of its components: Rayleigh molecules $\tau_{R\lambda}$, aerosols $\tau_{A\lambda}$, clouds $\tau_{C\lambda}$, and gas $\tau_{G\lambda}$. (Since $\tau_{C\lambda}$ only weakly varies with λ, we will drop the subscript λ, understanding that $\tau_C = \tau_{C,\lambda=0.55\ \mu m}$). We see that for a thin cloud (Fig. 3b) spectrally variable aerosol, air molecules, and gas dominate in the total optical depth and there are few spectral intervals where τ_λ does not vary over a large range. However, for thicker clouds ($\tau_C \geq 3$), a spectrally "flat" cloud dominates, making the total optical depth almost insensitive to spectral variations in $\tau_{R\lambda}$ and $\tau_{A\lambda}$ outside the water vapor absorbing bands. If strongly water vapor absorbing wavelengths are excluded, the extinction coefficient becomes weakly dependent on wavelength and the first condition for the applicability of SI stated in Eq. (5a) is approximately met.

The total asymmetry parameter of the scattering phase function (Fig. 4a) for optically thin clouds is strongly affected by molecular scattering, especially for shorter wavelengths. For thicker clouds, it exhibits much weaker variability with wavelength, suggesting that the second condition for SI, Eq. (5b), is also approximately met.

If the total extinction coefficient and the scattering phase function are only weakly dependent on wavelength, the spectral scattering and absorption processes in clouds are almost entirely determined by spectral variation in $\omega_{0\lambda}$ defined by Eq. (6b). Figure 4b shows $\omega_{0\lambda}$ for three cloud optical depths: $\tau_C = 0.5$, 3, and 10. Note that, in contrast to the cloud liquid water single scattering albedo that varies spectrally between 1 and 0.96 depending on droplet size, the total single scattering albedo is dominated by gaseous absorbing spectral bands and may fluctuate between 0 (gas only) and 1 (no absorption), especially for thinner clouds. This also suggests that while thick clouds suppress spectral variability in the total optical depth and scattering phase function, $\omega_{0\lambda}$ varies significantly because of its strong sensitivity to the absorbing and scattering properties of the atmospheric components. This feature makes it possible to implement the SI approach by directly relating radiative spectral properties of the atmosphere to the spectrum of $\omega_{0\lambda}$.

To increase the range of $\omega_{0\lambda}$ while keeping low spectral variation in τ_λ and g_λ, we will begin our analysis with only those wavelengths that have $\omega_{0\lambda} \geq 0.8$. Table 1 summarizes spectral variation in τ_λ and g_λ for those wavelengths. We can see that for $\tau_C \geq 3$, clouds suppress spectral sensitivity of τ_λ to $\tau_{R\lambda}$ and $\tau_{A\lambda}$ optical depths. As a result, for wavelengths with $\omega_{0\lambda} \geq 0.8$, the spectral variation in τ_λ and g_λ does not exceed 5% and 2%, respectively.

Finally we recall that Eq. (3) was derived under the assumption that the recollision and directional escape probabilities do not depend on the scattering order (see Fig. 1). In a general case, the spectral invariants vary with the number of successive collisions; however, they

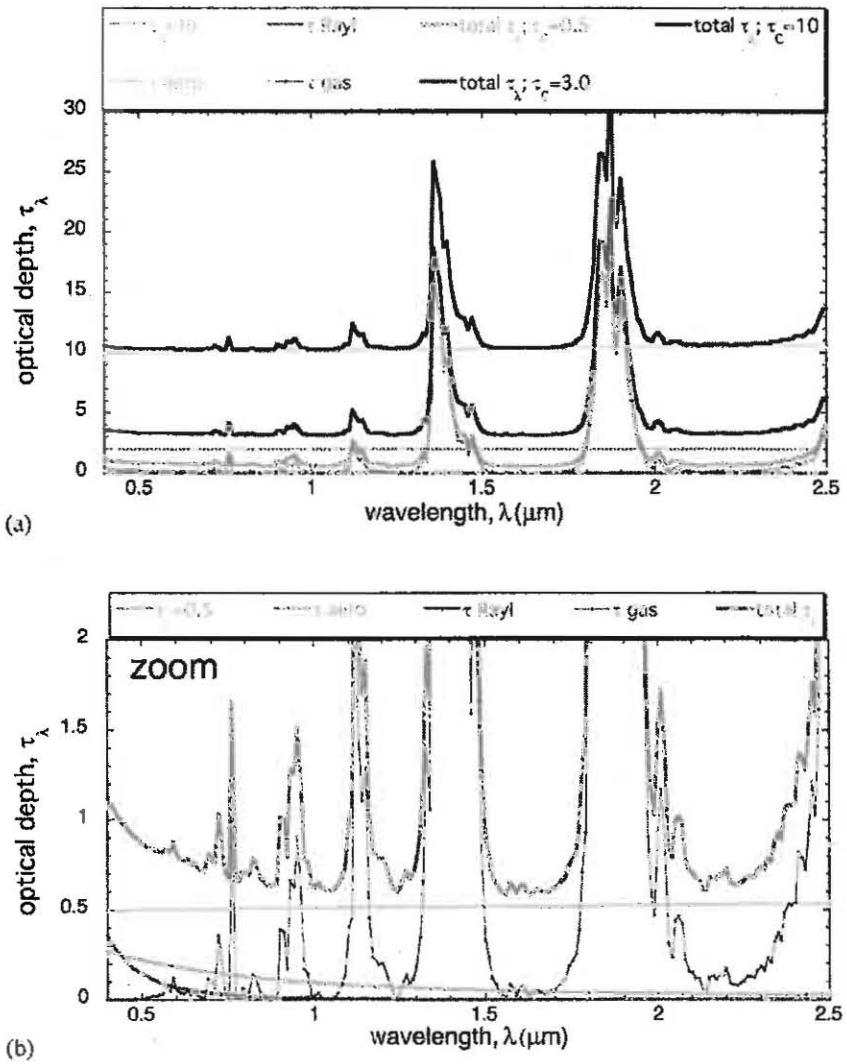

FIG. 3. Spectrum of total optical depth of a cloudy atmosphere as defined by Eq. (6d), accounting for air molecules (Rayleigh scattering), cloud droplets (scattering and absorption), aerosol particles (scattering and absorption), and gases (absorption). Optical depth of aerosol at $\lambda = 0.55$ μm is $\tau_A = 0.2$. (a) Three values of cloud optical depth: $\tau_C = 0.5$, 3, and 10 at $\lambda = 0.55$ μm. (b) Zoom of spectra for $\tau_C = 0.5$, cutting off at $\tau = 2$ as indicated by the dotted line in (a).

asymptote quickly as the number of collisions increases (Huang et al. 2007). For conservative scattering, Davis and Marshak (1997) estimated the number of forward scatterings required for particle to lose all memory of its original direction of travel as $(1 - g)^{-1} \approx 6$–7.

4. Radiative transfer calculations

To compute quantity $I_\lambda(\Omega)$ in Eq. (3) and its hemispherically integrated counterparts, the reflectance R_λ and transmittance T_λ, for wavelength range 0.4–2.5 μm with 10-nm resolution, we use the publicly available Santa Barbara DISORT Atmospheric Radiative Transfer (SBDART) code (Ricchiazzi et al. 1998) with a solar zenith angle of 45°. The other key parameters used in our simulations are listed in Table 2 and their choice is discussed in Chiu et al. (2010).

Let us come back to Eq. (3), multiply both sides by the cosine of a polar angle, and integrate over all 4π solid angle. Accounting for Eq. (2), we get

$$W_\lambda = \frac{(1 - p)\omega_{0\lambda}}{1 - p\omega_{0\lambda}}, \tag{7}$$

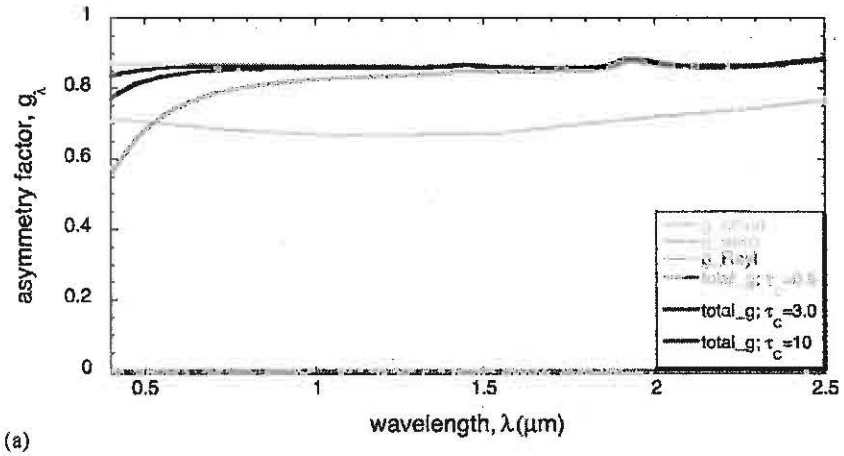

(a)

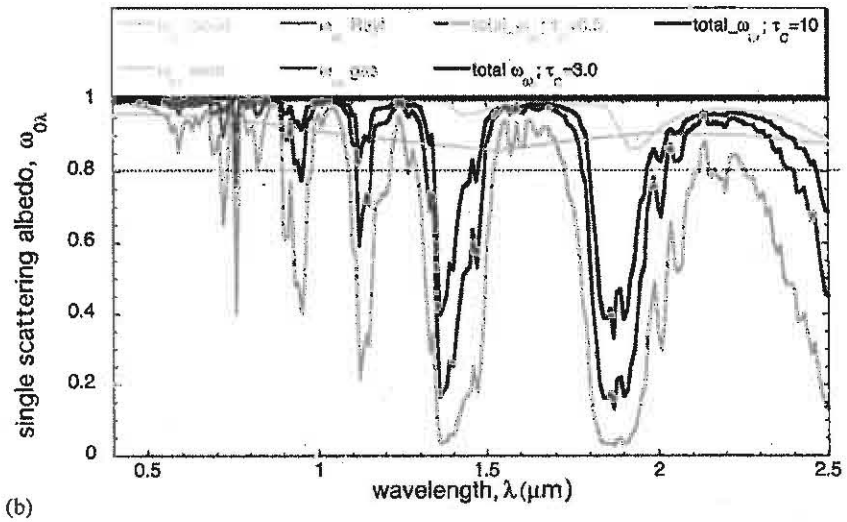

(b)

FIG. 4. (a) Spectra of g_λ for three cloud optical depths: $\tau_C = 0.5, 3$, and 10 with $\tau_{A,\lambda=0.55\mu m} = 0.2$. (b) Spectra of $\omega_{0\lambda}$ for the same three cases as in (a). See Eqs. (6b) and (6c) for definitions of "total" in each case.

where

$$W_\lambda(1 - T_{\text{dir}}) = R_\lambda + (T_\lambda - T_{\text{dir}}) \qquad (8a)$$

is the total radiation that has been reflected R_λ from, or diffusively transmitted $(T_\lambda - T_{\text{dir}})$ through, a cloudy layer. For sufficiently thick clouds the direct radiation $T_{\text{dir}} \approx 0$ and Eq. (8a) becomes

$$W_\lambda = R_\lambda + T_\lambda. \qquad (8b)$$

Here W_λ is the whole domain counterpart of $\omega_{0\lambda}$ while

$$A_{0\lambda} = 1 - W_\lambda$$

corresponds to the single scattering coalbedo $a_{0\lambda} = 1 - \omega_{0\lambda}$. From Eq. (7) we can prove that

$$W_\lambda \le \omega_{0\lambda}$$

because $p < 1$, and thus

$$A_{0\lambda} \ge a_{0\lambda}.$$

Interestingly, the $A_{0\lambda}$-to-$a_{0\lambda}$ ratio estimates the average number of photon interactions as a function of wavelength (Panferov et al. 2001; Knyazikhin et al. 2005):

$$n_\lambda = \frac{A_{0\lambda}}{a_{0\lambda}} = \frac{1 - W_\lambda}{1 - \omega_{0\lambda}} = \frac{1}{1 - p\omega_{0\lambda}} \ge 1. \qquad (9)$$

TABLE 1. Variations in the total optical depth and scattering phase function asymmetry parameter corresponding to wavelengths for which the single scattering albedo exceeds 0.8. The second row is for wavelengths between 0.7 and 2.5 μm. In the "$x \pm y$" notation in columns 3 and 5, x and y stand for the mean and the standard deviation, respectively.

Cloud optical depth	No. of wavelengths from 0.4 to 2.5 μm (out of total 210)	Total optical depth	Std dev to mean ratio for total optical depth (%)	Total asymmetry parameter	Std dev to mean ratio for total asymmetry parameter (%)
0.5	97	0.72 ± 0.12	17	0.79 ± 0.07	9
0.5	67	0.65 ± 0.05	8	0.83 ± 0.02	2
3	154	3.34 ± 0.16	5	0.85 ± 0.02	2
5	166	5.44 ± 0.24	4	0.86 ± 0.01	1
10	179	10.66 ± 0.44	4	0.86 ± 0.01	1

The final equality in Eq. (9) follows directly from Eq. (7). Note that the reciprocal of n_λ is linearly related to $\omega_{0\lambda}$. In addition, the product of n_λ and the photon mean free path $1/\sigma$ estimates the total photon path length:

$$L_\lambda = \frac{n_\lambda}{\sigma} = \frac{1}{\sigma}\frac{1}{1 - p\omega_{0\lambda}}. \tag{10}$$

Equation (10) shows the explicit dependence on p and allows us to estimate L_λ using explicit numerical models like SBDART [or the spherical harmonics discrete ordinate method (SHDOM); Evans 1998] rather than statistical models like Monte Carlo.

Figure 5 shows spectral variations of n_λ and W_λ. There are two remarkable points here. First, in the spectral interval 0.4–0.55 μm, n_λ increases from 17 to 23 for a thick cloud ($\tau_C = 10$) but slowly decreases for a thin one ($\tau_C = 0.5$). This behavior follows from the fact that for thicker clouds $\omega_{0\lambda}$ (Fig. 4b) decreases much more slowly than W_λ [see Fig. 5b and Eq. (10)], while for thin clouds, because of absorbing aerosols, $\omega_{0\lambda}$ decreases faster than W_λ. The recollision probability controls the response rate of W_λ to variation in $\omega_{0\lambda}$. The second remarkable point about Fig. 5 is the negligible effect of drop size except at wavelengths where liquid water absorbs strongly. In the spectral interval 2.1–2.2 μm, 16-μm droplets have an average of 13 photon interactions for $\tau_C = 10$, while for 4-μm (and therefore less absorbing) droplets, n_λ goes up to 18. Finally, for the strongly water vapor–absorbing spectral bands around 1.4 and 1.8 μm, $W_\lambda = 0$ and n_λ approaches 1.

Figure 6 plots points only for wavelengths for which $\omega_{0\lambda} > 0.8$ (see Table 1); there are 67 ($\tau_C = 0.5$), 154 ($\tau_C = 3.0$), and 179 ($\tau_C = 10.0$) such wavelength intervals. Figure 6a is similar to Fig. 5b. Figure 6b shows the ratio $W_\lambda/\omega_{0\lambda}$ plotted against W_λ, where the slope increases as we go from aerosol- and molecular-dominated conditions ($\tau_C = 0.5$) toward cloud-dominated conditions ($\tau_C = 3, 10$). The linear fit is almost perfect for $\tau_C = 10$. This confirms that SI holds for the cloud dominated cases—that is,

$$\frac{W_\lambda}{\varpi_{0\lambda}} = aW_\lambda + b \tag{11a}$$

or

$$W_\lambda = \frac{b\omega_{0\lambda}}{1 - a\omega_{0\lambda}}. \tag{11b}$$

Note that the sum of slopes a and intercepts b in Fig. 6b is almost exactly equal to unity. In the zero-absorption limit where the total $\omega_{0\lambda} = 1$, $W_\lambda = 1$ and consequently $a + b = 1$ from Eq. (11a).

Note that Eq. (11b) coincides with Eq. (7) if $a = p$ and $b = 1 - p$. Thus Fig. 6b numerically confirms the validity of Eq. (7). Finally, Eq. (11a) is equivalent to

TABLE 2. SBDART parameters.

Parameters	Values used in model
Spectral	
Lower wavelength limit	0.4 μm
Upper wavelength limit	2.5 μm
Spectral resolution	0.01 μm
Solar	
Solar spectrum	MODTRAN_3
Solar zenith angle	45°
Atmosphere	
Atmospheric profile	Midlatitude summer
Integrated water vapor amount	3 cm
Integrated ozone concentration	0.324 atm-cm
Surface	
Surface albedo	0
Cloud	
Cloud-base altitude	1 km
Cloud optical depth at 0.55 μm	0.0, 0.5, 3, 5, 10
Cloud drop effective radius	4 and 16 μm
Cloud phase function	Henyey–Greenstein
Aerosol	
Aerosol type	Rural
Aerosol optical depth at 0.55 μm	0.2
Aerosol phase function	Henyey–Greenstein
Visibility at 0.55 μm	23 km
Relative humidity used in the boundary layer aerosol model	80%

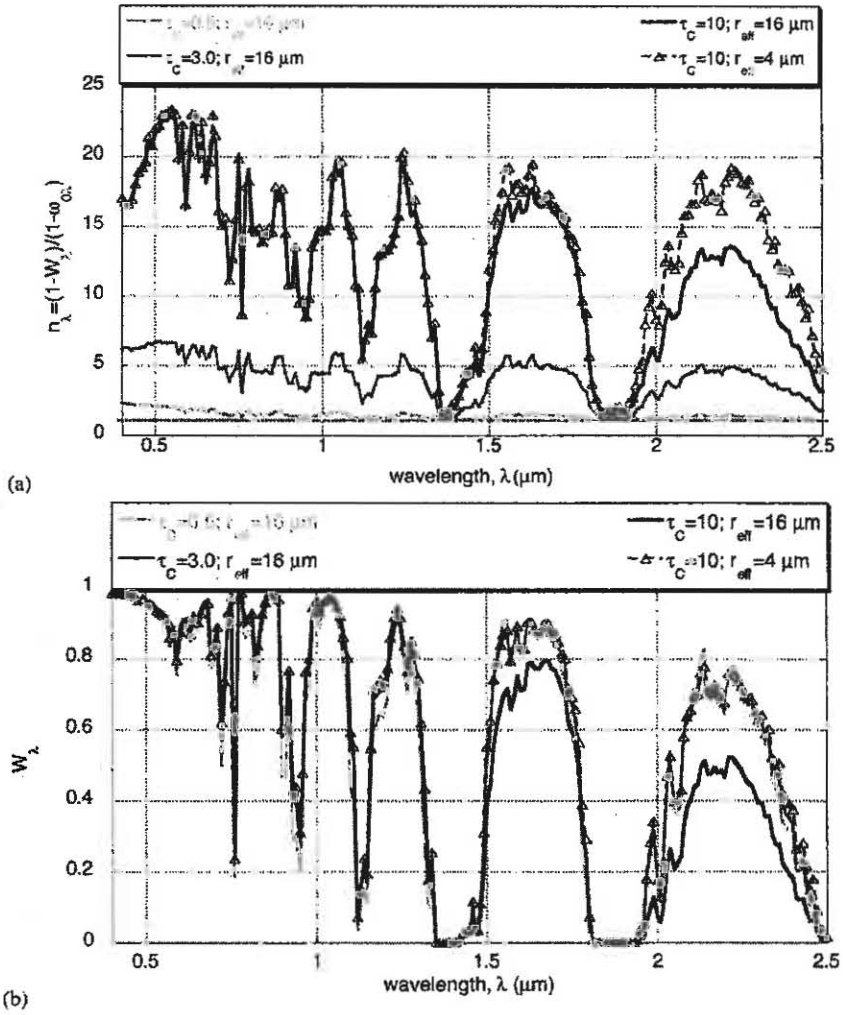

FIG. 5. (a) Spectra of estimates of n_λ for clouds with $\tau_C = 0.5, 3$, and 10 ($r_{\text{eff}} = 4$ and 16 μm); $\tau_{A,\lambda=0.55\mu m} = 0.2$. Dashed horizontal line corresponds to one interaction. (b) Spectra of W_λ for the same cases as in (a).

$$\frac{W_\lambda}{\omega_{0,\lambda}} = pW_\lambda + (1 - p). \tag{12}$$

Based on Eq. (12) the following interpretation of the linear relationship observed in Fig. 6b can be given. The terms $\omega_{0\lambda}$ and W_λ quantify the scattering events resulting from one and multiple interactions, respectively. Their ratio is the probability that a scattered photon will escape the layer as a result of multiple interactions. Part of the single scattered photons will escape without further interactions with the probability $(1 - p)$, and the rest with the probability pW_λ.

Interestingly, while both W_λ and $\omega_{0\lambda}$ depend on droplet radius (at least for the 2.1–2.2-μm spectral region, as seen in Fig. 5b), the slopes a (or p) are almost independent of droplet radius. Hence, the increase in n_λ for smaller droplets is due entirely to larger $\omega_{0\lambda}$, as follows from Eq. (9).

Finally, Fig. 7 shows the same kind of plot as in Fig. 6b, but for zenith and nadir radiances instead of W_λ. We see that (i) again, the behavior is very close to linear, at least for the cloud-dominated cases; (ii) for $\tau_C = 10$ the slopes for W_λ and for the two radiances are almost identical, while for the other cases the slopes are different; and (iii) the sum of a and b is not necessarily equal to 1.

In summary, for the cloud-dominated cases, both radiance and fluxes show evidence of SI as predicted by Eqs. (4) and (12).

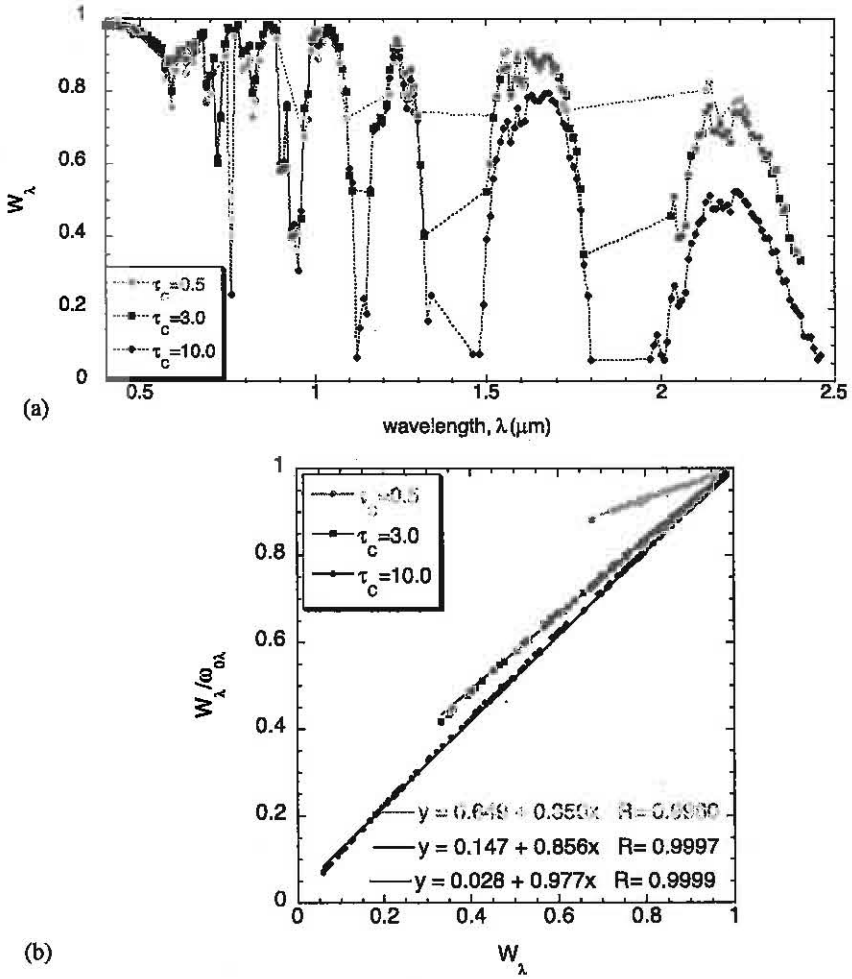

FIG. 6. (a) Spectra of W_λ for clouds with $\tau_C = 0.5, 3$, and 10 ($r_{\text{eff}} = 16$ μm); $\tau_{A,\lambda=0.55\mu\text{m}} = 0.2$. Doglegs occur because only wavelengths for which $\omega_{0\lambda} > 0.8$ (see Table 1) are plotted. (b) Ratio $W_\lambda/\omega_{0\lambda}$ is plotted against W_λ for the wavelengths from (a). To reduce variability in τ_λ and g_λ (see Table 1), wavelengths less than 0.7 μm were not used for $\tau_C = 0.5$.

5. Accuracy of the spectrally invariant relationships

To address the question of accuracy in the SI relationships, we first introduce a more accurate wavelength-selection method than the criterion $\omega_{0\lambda} > 0.8$ (Table 1) used in section 3. This method will be applied to obtain the slope and intercept. Second, we reconstruct the radiance spectra using the single scattering albedo and SI parameters and compare them with those calculated with the SBDART code.

Solving Eq. (7) for p yields

$$p_\lambda = \frac{\omega_{0\lambda} - W_\lambda}{\omega_{0\lambda}(1 - W_\lambda)}. \tag{13}$$

Our goal is to find the spectral intervals for which variation in p_λ is small. Figure 8a shows variation in p_λ with wavelength. The sharp peaks around the absorbing bands are correlated with the total optical depth (cf. Fig. 3). In the spectral interval between 0.4 and 0.55 μm, p_λ increases for thick clouds ($\tau_C \gtrsim 3$) and decreases for a thin one ($\tau_C = 0.5$). For $\lambda \geq 0.55$ μm, p_λ becomes relatively flat outside the absorbing bands. Figure 8b shows the occurrences of the p_λ values from Fig. 8a while Tables 3 and 4 summarize their statistics for wavelengths corresponding to the maxima in Fig. 8b. For such wavelengths, the $W_\lambda/\omega_{0\lambda}$ versus W_λ relationships are more linear than the $I_\lambda/\omega_{0\lambda}$ versus I_λ relationships and their sums of slope and intercept are closer to unity. The tables show that the statistics of frequency peaks is only weakly sensitive to cloud drop size (as can be seen also in Fig. 8b).

Equations (3) and (7) can be combined as

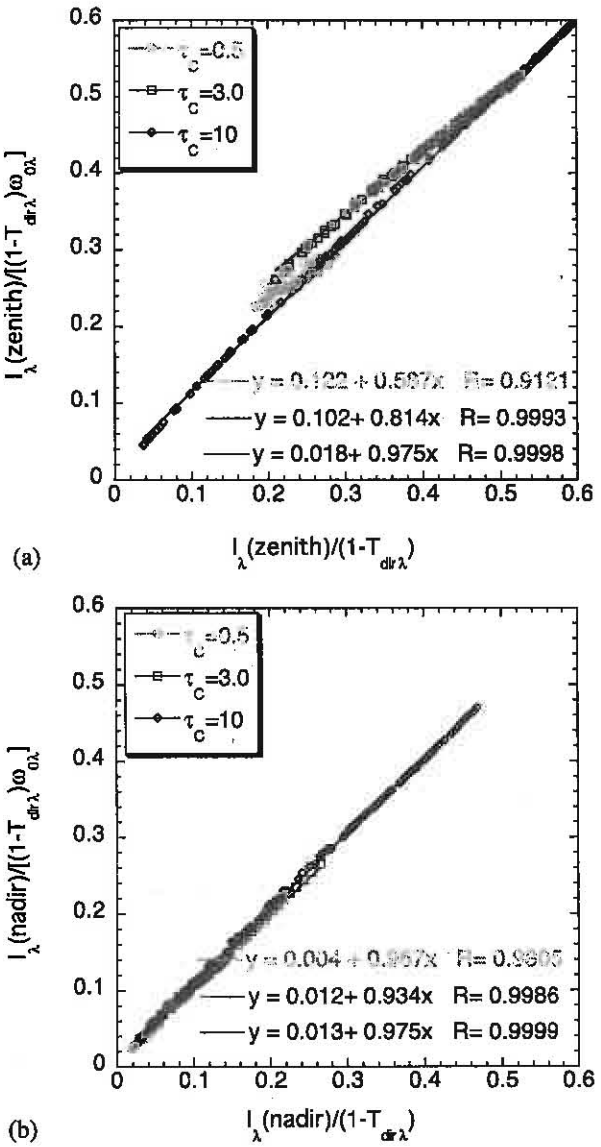

FIG. 7. As in Fig. 6b, but for (a) $I_\lambda(\Omega)$ in zenith ($\Omega = \downarrow$) direction and (b) $I_\lambda(\Omega)$ in nadir ($\Omega = \uparrow$) direction, where I is reflected radiance.

$$\frac{I_\lambda(\Omega)}{1 - T_{\text{dir}}} = \kappa(\Omega) W_\lambda, \tag{14a}$$

which, using Eq. (8a), is equivalent to

$$I_\lambda(\Omega) = \kappa(\Omega)(R_\lambda + T_\lambda - T_{\text{dir}}), \tag{14b}$$

where $\kappa(\Omega) = \rho(\Omega)/(1 - p)$ maps the total diffuse outgoing flux into radiance [see Eq. (2)]. If the optical depth and the scattering phase function are independent of wavelength, the coefficient κ does not depend on wavelength either and varies with Ω (and the direction of incident radiation Ω_0). Its physical interpretation is similar to the scattering phase function but formulated for the entire layer (i.e., the fraction κ of scattered photons W_λ leaves the layer in a given Ω). Figure 9 shows occurrence of κ values for nadir radiance. Unlike p values, κ maxima become very sensitive to the drop sizes. If one selects only wavelengths that correspond to the maxima of both p and κ, the differences in slopes between the two cases (hemispherical and directional) will be much smaller, as the theory predicts.

Figure 10a illustrates the improvement of the linearity in the $W_\lambda/\omega_{0\lambda}$ versus W_λ relationships with rejection of wavelengths, where τ_λ substantially fluctuates (see Fig. 3a). In addition to our standard case of $\omega_{0\lambda} > 0.8$ with 179 wavelengths (Table 1), we also plotted the $\omega_{0\lambda}$ thresholds of 0.9 with 156 wavelengths. As expected, the increased $\omega_{0\lambda}$ threshold slightly improves the regression coefficient and decreases the slope (thus increasing the intercept).

The improved linearity makes the reconstruction of W_λ more accurate, especially for the shorter wavelengths (Fig. 10b). However, further increase in the threshold does not necessarily improve the accuracy. This is due to the reduced information on cloud liquid water absorption by removing longer wavelengths (around 1.6 and, especially, 2.1 μm). Figure 11 illustrates the RMS and the bias

$$\text{RMS} = \sqrt{\frac{1}{m}\sum_{i=1}^{m}(W_{i,\lambda} - W_{i,\lambda,\text{appr}})^2} \tag{15a}$$

$$\text{bias} = \frac{1}{m}\sum_{i=1}^{m} W_{i,\lambda} - \frac{1}{m}\sum_{i=1}^{m} W_{i,\lambda,\text{appr}} \tag{15b}$$

for 10 approximations corresponding to the increased $\omega_{0\lambda}$ thresholds ($m = 211$). We see that there are few changes for the thresholds above $\omega_{0\lambda} = 0.97$. This is because most of the cloud liquid water absorbing wavelengths around 2.1 μm have been removed and the range of $\omega_{0\lambda}$ has been substantially decreased. The best approximation is reached for the thresholds of 0.86 and 0.92–93 for the bias and the RMS, respectively. Note that the threshold that gives the minimum RMS is very close to the one that is based on the maximum p values occurrence (see Table 4).

What is the optimal number of wavelengths needed to obtain the recollision probability and what are those wavelengths? To increase the dynamic range of ω_0 and thus the corresponding range of the I/ω_0 versus I scatterplot, one needs to use wavelengths with the largest range of cloud water absorption. In Fig. 12a we used three wavelengths: 0.4 μm (total $\omega_0 = 0.999$, $\tau = 10.57$,

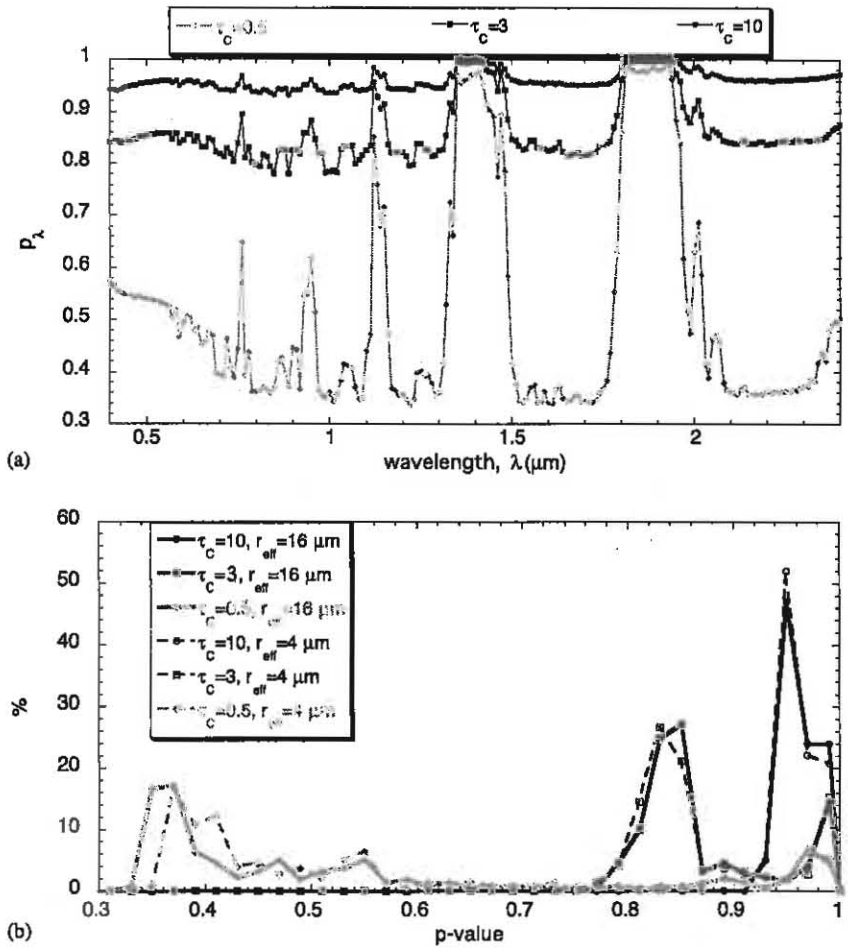

FIG. 8. (a) Spectra of p_λ for $\tau_C = 0.5, 3$, and 10; $r_{\text{eff}} = 16$ μm. (b) Histograms of p_λ from (a) for $r_{\text{eff}} = 4$ and 16 μm with bin width 0.02.

$g = 0.835$), 1.6 μm ($\omega_0 = 0.982, \tau = 10.46, g = 0.861$), and 2.1 μm ($\omega_0 = 0.948$, $\tau = 10.66$, $g = 0.866$). The reconstructed W_λ for all wavelengths from 0.4 to 2.5 μm is shown in Fig. 12b. The RMS = 0.046 (~9% of the mean value of $W_\lambda = 0.53$) and the bias = −0.006. Note that accuracy of the approximation is not very sensitive to a selection of a particular wavelength in the neighborhoods of 0.4, 1.6, and 2.1 μm. Finally, it seems

TABLE 3. Statistics of the "p_λ peak" values from Fig. 8b for $r_{\text{eff}} = 4$ μm. Bin size is 0.02. The cloud-free column ($\tau_C = 0.0$) is added for comparison. "Var" indicates coefficient of variation (the ratio of the standard deviation to the mean).

Parameters	Cloud optical depth (droplet size $r_{\text{eff}} = 4$ μm)				
	0.0	0.5	3.0	5.0	10.0
Bin	0.02–0.04	0.36–0.38	0.82–0.84	0.90–0.92	0.94–0.96
No. of points	27	37	59	71	115
Mean p	0.030	0.371	0.832	0.910	0.950
Var p (%)	17.0	1.4	0.7	0.6	0.6
Min $\omega_{0\lambda}$	0.163	0.722	0.873	0.884	0.937
Max $\omega_{0\lambda}$	0.655	0.963	0.998	0.998	0.999
Var $\omega_{0\lambda}$ (%)	47.4	7.8	3.9	3.1	1.4
Min τ_λ	0.072	0.630	3.22	5.27	10.32
Max τ_λ	0.170	0.829	3.90	6.90	12.51
Var τ_λ (%)	24.7	8.7	5.8	8.6	5.5
Correlation coefficient R^2 of linear relationship	0.673 22	0.998 63	0.999 85	0.999 89	0.999 91

TABLE 4. As in Table 3, but for $r_{eff} = 16$ μm. "Var" indicates coefficient of variation (the ratio of the standard deviation to the mean).

Parameters	Cloud optical depth (droplet size $r_{eff} = 16$ μm)				
	0.0	0.5	3.0	5.0	10.0
Bin	0.02–0.04	0.36–0.38	0.82–0.84	0.90–0.92	0.94–0.96
No. of points	27	38	65	72	104
Mean p	0.030	0.367	0.832	0.909	0.950
Var p (%)	17.0	1.4	0.7	0.5	0.6
Min $\omega_{0\lambda}$	0.163	0.683	0.868	0.869	0.937
Max $\omega_{0\lambda}$	0.655	0.964	0.997	0.998	0.999
Var $\omega_{0\lambda}$ (%)	47.4	10.9	3.7	3.6	1.5
Min τ_λ	0.072	0.587	3.15	5.21	10.2
Max τ_λ	0.170	0.818	3.16	5.95	11.0
Var τ_λ (%)	24.7	10.3	3.8	2.9	1.5
R^2 of linear relationship	0.673 22	0.998 94	0.999 86	0.999 91	0.999 91

counterintuitive that the case with only three selected wavelengths (Fig. 12b) gives a better approximation than the one that uses more than 100 wavelengths (Fig. 11). However, the case with a large number of wavelengths is biased toward the visible spectral interval at the expense of near-infrared wavelengths. In addition, using a larger number of wavelengths leads to more violations of the assumptions stated in Eqs. (5a) and (5b). Thus more wavelengths do not necessarily provide a better approximation.

6. Possible applications

Guided by applications already being pursued in vegetation canopy radiative transfer (Ganguly et al. 2008; Schull et al. 2011) we think the top applications are (i) testing the consistency of remote sensing retrievals, (ii) broadband calculations for climate models, (iii) filling missing spectral data, and (iv) testing 3D radiative transfer codes. Below we briefly discuss all four.

a. Testing the consistency of remote sensing retrievals

Satellite remote sensing often provides particle effective radius r_{eff} at three liquid water absorbing wavelengths: 1.6, 2.1, and 3.7 μm. From r_{eff} one can calculate the "effective" $\omega_{0\lambda}$ for each wavelength. Now Eq. (4) can be used to validate the physical consistency of the retrieved r_{eff} values. Indeed, according to the SI theory, the ratio of I_λ to $\omega_{0\lambda}$ should be approximately linear in I_λ. Lack of linearity may call into question the correctness of retrievals.

b. Broadband calculations for climate models

For climate models it is assumed that if r_{eff} is known, the total $\omega_{0\lambda}$ can be calculated (or parameterized; see, e.g., Slingo 1989) as a function of wavelength (or spectral band). Using the assumptions of the SI approach, one can calculate fluxes for only a few (at least, two or three) wavelengths and obtain the two wavelength-independent variables (a and b). Fluxes for all other wavelengths could

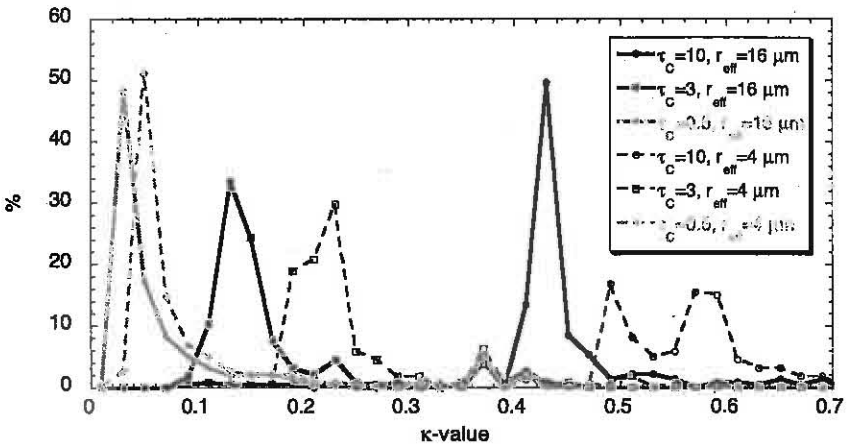

FIG. 9. As in Fig. 8b, but for κ values. The term $\kappa(\Omega) = \rho(\Omega)/(1 - p)$ maps the total diffuse outgoing flux into radiance. Also, p and $\rho(\Omega)$ are the recollision probability and the directional escape probability, respectively [see Eq. (2)].

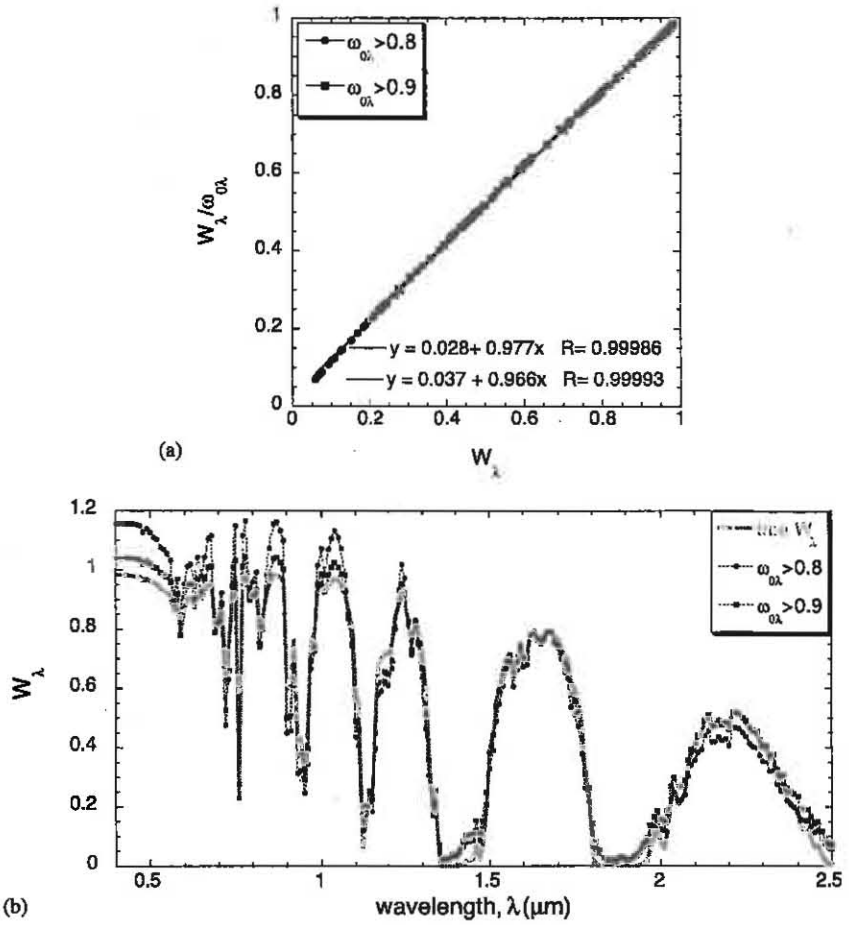

FIG. 10. (a) Relationships of $W_\lambda/\omega_{0\lambda}$ vs W_λ for wavelengths such that $\omega_{0\lambda} > 0.8$ (179 values) and $\omega_{0\lambda} > 0.9$ (156 values). Other parameters are $\tau_C = 10$, $r_{\text{eff}} = 16$ μm, $\tau_{A,\lambda=0.55\mu m} = 0.2$. (b) Reconstruction of W_λ using Eq. (11b), where slopes and intercepts are from the linear relationships in (a). All 211 wavelengths from 0.4 to 2.5 μm are retrieved.

be derived from these two variables and $\omega_{0\lambda}$. Thus for estimating a broadband integral, a small number of radiative transfer calculations may be sufficient if high accuracy is not required. Note that $W_\lambda = 1 - A_\lambda$ has been approximated as a function of all shortwave wavelengths from 0.4 to 2.5 μm using radiative transfer calculations at only three wavelengths (see Fig. 12b) with a bias of 0.006 out of 0.53 or 1.1%. However, if both the broadband R_λ and T_λ are required, the biases will be bigger.

c. *Filling missing spectral data*

When high temporal and spectral resolution radiance measurements are provided by an aircraft spectrometer, some spectral data may be lost because of saturation or transmission problems (A. Vogelmann 2010, personal communication). In this case, if the SI relationship is established and the SI variables are found, the lost spectral data can be reconstructed using Eq. (4).

d. *Testing 3D radiative transfer codes*

The best way to test a new numerical radiative transfer model is to compare its results with a nontrivial exact solution of the radiative transfer equation. Unfortunately, few such solutions are available, especially for 3D radiative transfer. To compare different atmospheric radiative transfer models, the Intercomparison of 3D Radiation Codes (I3RC; see http://i3rc.gsfc.nasa.gov and Cahalan et al. 2005) used some "consensus" results. To replace the unavailable "truth" for the Radiation Transfer Model Intercomparison (RAMI) in vegetation, Pinty et al. (2001, 2004) introduced the "most credible solution." However, both intercomparisons of radiation codes (I3RC and RAMI) mostly compared the

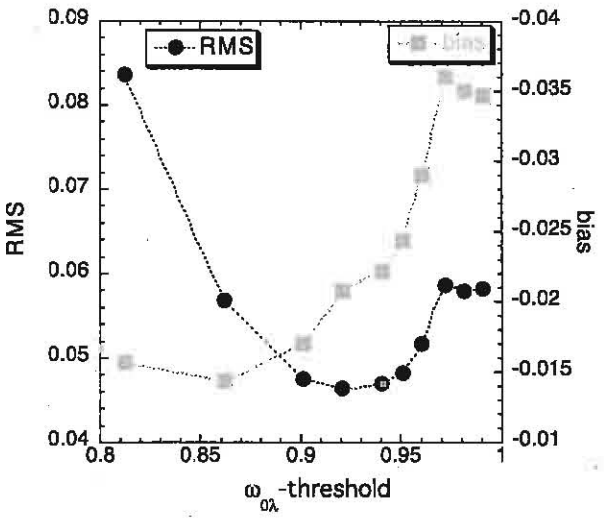

FIG. 11. RMS and bias [see Eq. (15) with $n = 211$] of W_λ for different approximations based on $\omega_{0\lambda}$ thresholds.

model results against each other. The SI theory suggests a more robust physics-based approach for testing radiative transfer codes. This approach states that the ratios of the calculated radiative quantities (radiances and/or fluxes) to the spectral single scattering albedo for three or more wavelengths are expected to be approximately linear in these radiative quantities.

Note that the direct application of the SI relationships is limited only to cases with a purely absorbing surface. However, the relationships are an important part of the radiative transfer problem with general boundary conditions (see the appendix). More studies are needed to better understanding the limitations of applicability of the SI relationships to real atmospheres.

7. Summary and discussion

The solution of the radiative transfer equation depends on its boundary conditions (solar illumination and surface reflectance) and on three (independent) variables—optical depth τ_λ, phase function P_λ, and single scattering albedo $\omega_{0\lambda}$. We assume that the functional dependence of the solution of the radiative transfer equation I_λ on $\{\tau_\lambda, P_\lambda\}$ does not change with wavelength while the wavelength dependence of I_λ comes only from the $\omega_{0\lambda}$ spectra. In this case, we can formally write

$$I_\lambda(\tau_\lambda, P_\lambda \omega_{0\lambda}) = I_\lambda(\tau, P; \omega_{0\lambda}). \tag{16}$$

Such a separation of variables is natural for radiative transfer in leaf canopies where scattering centers are much larger than the wavelength of solar radiation and dependence on τ and P is determined by canopy structure while dependence on $\omega_{0\lambda}$ comes entirely from leaf physiology.

For atmospheric radiative transfer this assumption is not met, in general (see Figs. 3a,b and 4a), since the size of scattering centers (air molecules, aerosol and cloud particles) is comparable to (or smaller than) the wavelength of solar radiation.

However, in cloudy atmospheres assumption (16) can be met approximately for a large range of wavelengths. This paper shows that, at least for $\tau_C \geq 3$ and wavelengths that exclude strong water vapor absorbing spectral intervals, Eqs. (5a) and (5b) hold with variations less than 5% (Table 1). Consequently, the linear spectral-invariant relationships are valid (see Figs. 6b and 7a,b); that is, the ratio of the radiative quantity (radiance or flux) to the total single scattering albedo is a linear function of this quantity; its slope and intercept are wavelength independent.

The slope of the linear function is an approximation to the recollision probability—the probability that a scattered photon will interact with the medium again. The intercept of the linear function quantifies the escape probability in a given direction. For hemispherically integrated fluxes [Eqs. (8a) and (8b)], the sum of the slope and the intercept is equal to one [see Eqs. (7) and (12) and Fig. 6b]; this is not necessarily true for radiances (Figs. 7a,b).

The ratio of the absorbed radiation to the single scattering coalbedo estimates the number of interactions; the reciprocal of the number of interactions is linearly related to the single scattering albedo [Eq. (9)]. As a function of wavelength, the total photon path length can be estimated [Eq. (10)] using explicit numerical radiative transfer models such as SBDART for 1D and SHDOM for 3D calculations.

The results presented in the paper can be directly applied to simple radiative transfer calculations if the same radiative quantity is required for different single scattering albedos (see Figs. 2a,b). In brief, we were able to single out one spectral variable—the single scattering albedo—that determines spectral behavior. If the single scattering albedo is known, it will help to fill spectral gaps in the spectral observations. In addition, the possible applications of SI to climate and remote sensing research are summarized in section 6.

If the spectral single scattering albedo is available, the slope of the linear relationship can be obtained directly from observations without any parameterizations and/or radiative transfer calculations. The product of the slope (the recollision probability) and the single scattering albedo approximates the maximum eigenvalue of the radiative transfer equation (see the appendix). As far as we

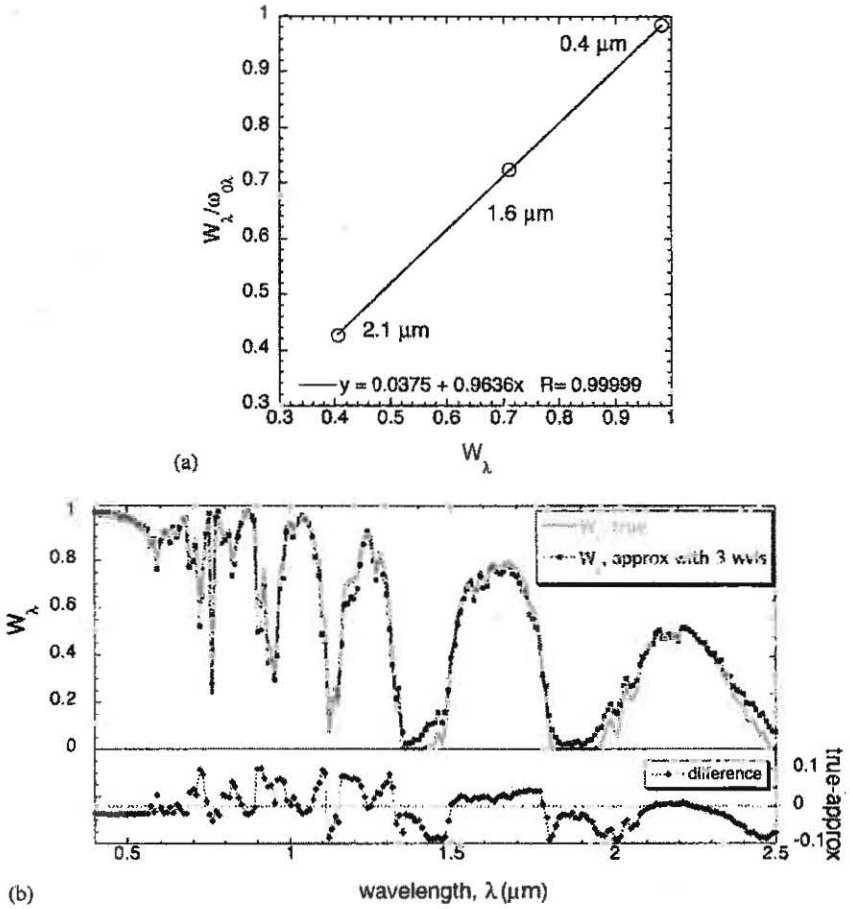

FIG. 12. (a) Relationships of $W_\lambda/\omega_{0\lambda}$ vs W_λ for $\lambda = 0.4, 1.6$, and 2.1 μm. Other parameters are $\tau_C = 10$, $r_{\text{eff}} = 16$, $\tau_{A,\lambda=0.55\mu m} = 0.2$. (b) Reconstruction of W_λ using Eq. (11a) or (7) with slope (as p) and intercept (as $1 - p$) obtained from (a). Retrieved values for all 211 wavelengths from 0.4 to 2.5 μm are shown.

are aware, this is the first method for estimating the maximum eigenvalue directly from atmospheric measurements.

The concept of collision and escape probabilities was first introduced and developed in nuclear reactor physics (Bell and Glasstone 1970, 115–125). The vegetation community used this concept to interpret the SI relationships observed in radiative measurements and satellite data and to relate the wavelength-independent recollision and escape probabilities to canopy structure. In this paper the principles of SI have been applied to atmospheric radiative transfer. This provides a bridge between the methods developed in reactor physics, vegetation canopies, and cloudy atmospheres since all three use the same radiative transfer equation.

Finally, recently Marshak et al. (2009) reported a surprising SI relationship in shortwave spectrometer observations taken by the Atmospheric Radiation Measurement program (ARM). The relationship suggests that the shortwave spectrum near cloud edges can be determined by a linear combination of zenith radiance spectra of the cloudy and clear regions. Chiu et al. (2010) confirmed these findings with intensive radiative transfer simulations of the different aerosols and clouds properties as well as the underlying surface types, and the finite field of view of the spectrometer. Although their calculations are performed for 1D clouds, the first 3D radiative transfer results suggest that the SI relationship discovered in shortwave spectrometer measurements is valid for the 3D simulation world. However, the slope and intercept depend on cloud structure and may be different from their 1D counterparts. A clear physical (and mathematical) understanding of the observed and simulated SI behavior of zenith radiance around cloud edges is still missing. The current paper is the first step in this direction.

Acknowledgments. This research was supported by the Office of Science (BER, U.S. Department of Energy, Interagency Agreements DE-AI02-08ER64562, DE-FG02-08ER64563, and DE-FG02-08ER54564) as part of the ARM program. We also thank A. Davis, F. Evans, A. Lyapustin, L. Oreopoulos, P. Pilewskie, R. Pincus, S. Schmidt, A. Vasilkov, and Z. Zhang for fruitful discussions.

APPENDIX

Eigenvalues of the Radiative Transfer Equation and Spectral Invariance

a. Definition

An eigenvalue of the 3D radiative transfer equation is a number γ such that there exists a nontrivial function $e(x, \Omega)$ that satisfies the equation

$$\gamma[\Omega \cdot \nabla e(x, \Omega) + \sigma(x) e(x, \Omega)] = \int_{4\pi} \sigma_{s,\lambda}(\Omega' \to \Omega) e(x, \Omega')\, d\Omega', \quad \text{(A1)}$$

and zero boundary conditions. The 3D radiative transfer equation has a discrete set of eigenvalues γ_k and eigenvectors $e_k(x, \Omega)$, $k = 0, 1, 2, \ldots$. Under some general conditions, the eigenvectors are mutually orthogonal. Solution of the radiative transfer equation can be expanded in eigenvectors. There is a positive eigenvalue γ_0 that corresponds to a positive eigenvector $e_0(x, \Omega)$. The eigenvalue γ_0 is greater than the absolute magnitudes of the remaining eigenvalues. It means that this eigenvalue and corresponding eigenvector dominates all other eigenvalues and eigenvectors. The reciprocal of the positive eigenvalue γ_0 describes the criticality condition in reactor physics—that is, a relation between $1/\gamma_0$ and the size of the assembly when more than one neutron is emitted per collision (Bell and Glasstone 1970; Case and Zweifel 1967). Details of this theory can be found in Vladimirov (1963) and Knyazikhin et al. (2011).

The positive eigenvalue γ_0 and corresponding eigenvector e_0 have the following interpretation. Equation (A1) can be rewritten in terms of linear operators: differential operator L [the square brackets of Eq. (A1)] and integral operator S [the right-hand side of Eq. (A1)], as $\gamma_0 L e_0 = S e_0$. Solving this equation for γ_0 yields $\gamma_0 = L^{-1} S e_0 / e_0$. The operator $L^{-1}S$ inputs the source e_0, simulates the scattering event S and the photon free path L^{-1}, and outputs the distribution of photons just before their next interaction. The ratio $L^{-1} S e_0 / e_0$ therefore can be treated as the probability that a scattered photon will recollide.

b. Conditions for wavelength independency

In cloudy atmospheres, the scattering coefficient $\sigma_{s,\lambda} = \omega_{0\lambda} \sigma P$, where $\omega_{0\lambda}$ and P are the single scattering albedo and scattering phase function, respectively. The scattering operator S takes the form $S = \omega_{0\lambda} S_0$, where S_0 is determined by the extinction coefficient σ and P. Equation (A1) can be rewritten as $pLe = S_0 e$, where $p = \gamma/\omega_{0\lambda}$ is the probability that a scattered photon will recollide. If the extinction coefficient and scattering phase function do not depend on wavelength, L and S_0 are wavelength independent. As a result, the recollision probability becomes wavelength independent and does not depend on the incoming radiation either.

c. Comments on Eq. (3)

The 3D radiative transfer equation with a nonreflecting boundary can be transformed into the integral equation

$$I_\lambda = \omega_{0\lambda} T_0 I_\lambda + Q, \quad \text{(A2)}$$

where $T_0 = L^{-1} S_0$; the source term Q describes the distribution of uncollided radiation. The operator T_0 has the same set of eigenvalues and eigenvectors as Eq. (A1), i.e., $\gamma_k e_k = \omega_{0\lambda} T_0 e_k$. If σ does not depend on wavelength, Q becomes wavelength independent. In addition, if P does not vary with wavelength, T_0 becomes spectrally invariant. Solution of the radiative transfer equation can be expanded in successive order of scattering, which has a form of series similar to Eq. (3); that is, the terms in series (3) are powers of T_0 that are proportional to $\rho \omega_{0\lambda}^m p^{m-1}$. More details on relationships among T_0, recollision, and escape probabilities as well as their dependences on the scattering order m can be found in Huang et al. (2007).

Note that the concept of spectral invariance is formulated for a medium bounded by a nonreflecting surface. The 3D radiative transfer problem with arbitrary boundary conditions can be expressed as a superposition of the solutions of some basic radiative transfer subproblems with purely absorbing boundaries (Davis and Knyazikhin 2005) to which the spectral invariants are applicable.

d. Number of interactions

The mean number of photon interactions N_λ is an important variable characterizing the effect of multiple scattering on the atmosphere reflective and absorptive properties. This is just the integral of σI over spatial and angular variables; that is,

$$N_\lambda = \|I_\lambda\| = \int_{4\pi}\int_V \sigma(x) I_\lambda(x,\Omega)\, dx\, d\Omega \quad \text{(A3)}$$

over a domain V. Multiplying Eq. (A2) by σ and integrating over spatial and angular variables yields

$$N_\lambda = \omega_{0\lambda}\frac{\|T_0 I_\lambda\|}{\|I_\lambda\|}N_\lambda + i_0. \quad \text{(A4)}$$

Here $i_0 = \int_{4\pi}\int_V \sigma(x)Q(x,\Omega)\, dx\, d\Omega = 1 - T_{\text{dir}}$, where T_{dir} is the directly transmitted radiation (section 4). Neglecting all terms in the expansion of the solution of the radiative transfer equation in eigenvectors except the dominant one e_0, one gets $\|T_0 e_0\|/\|e_0\| \approx p$. Substituting it into Eq. (A4) and normalizing by i_0, one obtains Eq. (9), where $n_\lambda = N_\lambda/i_0$. Given N_λ, the absorption can be estimated as $(1 - \omega_{0\lambda})N_\lambda$. More details can be found in Panferov et al. (2001) and Knyazikhin et al. (2011).

e. Energy conservation law

Let A_λ and $S_\lambda = R_\lambda + T_\lambda - T_{\text{dir}}$ be fractions of photons from the incident beam that are absorbed and diffusely scattered (reflected or transmitted) out by the layer, respectively. The energy conservation law takes the form (Smolander and Stenberg 2005)

$$A_\lambda + R_\lambda + T_\lambda = A_\lambda + S_\lambda + T_{\text{dir}} = 1. \quad \text{(A5)}$$

The diffusely scattered radiation is then

$$S_\lambda = (1 - T_{\text{dir}}) - (1 - \omega_{0\lambda})n_\lambda i_0 = \frac{(1-p)\omega_{0\lambda}}{1 - p\omega_{0\lambda}} i_0. \quad \text{(A6)}$$

Equation (7) for the layer scattering $W_\lambda = S_\lambda/i_0$ directly follows from Eq. (A6). [Note that A_λ in Eq. (A5) and $A_{0\lambda}$ in Eq. (9) are different by a factor of i_0.]

REFERENCES

Bell, G. I., and S. Glasstone, 1970: *Nuclear Reactor Theory*. Van Nostrand Reinholt, 619 pp.

Cahalan, R. F., and Coauthors, 2005: The I3RC: Bringing together the most advanced radiative transfer tools for cloudy atmospheres. *Bull. Amer. Meteor. Soc.*, **86,** 1275–1293.

Case, K. M., and P. F. Zweifel, 1967: *Linear Transport Theory*. Addison Wesley, 342 pp.

Chiu, J. C., A. Marshak, Y. Knyazikhin, and W. J. Wiscombe, 2010: Spectrally-invariant behavior of zenith radiance around cloud edges simulated by radiative transfer. *Atmos. Chem. Phys.*, **10,** 11 295–11 303.

Davis, A., and A. Marshak, 1997: Lévy kinetics in slab geometry: Scaling of transmission probability. *Fractal Frontiers,* M. M. Novak and T. G. Dewey, Eds., World Scientific, 63–72.

——, and Y. Knyazikhin, 2005: Three-dimensional radiative transfer in the cloudy atmosphere. *A Primer in Three-Dimensional Radiative Transfer,* A. Marshak and A. B. Davis, Eds., Springer-Verlag, 153–242.

Evans, K. F., 1998: The spherical harmonics discrete ordinate method for three-dimensional atmospheric radiative transfer. *J. Atmos. Sci.*, **55,** 429–446.

Ganguly, S., A. Samanta, M. A. Schull, N. V. Shabanov, C. Milesi, R. R. Nemani, Y. Knyazikhin, and R. B. Myneni, 2008: Generating vegetation leaf area index Earth system data record from multiple sensors. Part 2: Implementation, analysis and validation. *Remote Sens. Environ.*, **112,** 4318–4332.

Huang, D., and Coauthors, 2007: Canopy spectral invariants for remote sensing and model applications. *Remote Sens. Environ.*, **106,** 106–122.

Knyazikhin, Y., J. V. Martonchik, R. B. Myneni, D. J. Diner, and S. W. Running, 1998: Synergistic algorithm for estimating vegetation canopy leaf area index and fraction of absorbed photosynthetically active radiation from MODIS and MISR data. *J. Geophys. Res.*, **103,** 32 257–32 275.

——, A. Marshak, and R. B. Myneni, 2005: Three-dimensional radiative transfer in vegetation canopies and cloud–vegetation interaction. *Three-Dimensional Radiative Transfer in the Cloudy Atmosphere,* A. Marshak and A. B. Davis, Eds., Springer-Verlag, 617–652.

——, M. A. Schull, L. Xu, R. B. Myneni, and A. Samanta, 2011: Canopy spectral invariants. Part 1: A new concept in remote sensing of vegetation. *J. Quant. Spectrosc. Radiat. Transfer,* **112,** 727–735.

Marshak, A., Y. Knyazikhin, J. C. Chiu, and W. J. Wiscombe, 2009: Spectral invariant behavior of zenith radiance around cloud edges observed by ARM SWS. *Geophys. Res. Lett.*, **36,** L16802, doi:10.1029/2009GL039366.

Nakajima, T., and M. D. King, 1990: Determination of the optical thickness and effective particle radius of clouds from reflected solar-radiation measurements. 1. Theory. *J. Atmos. Sci.*, **47,** 1878–1893.

Panferov, O., Y. Knyazikhin, R. B. Myneni, J. Szarzynski, S. Engwald, K. G. Schnitzler, and G. Gravenhorst, 2001: The role of canopy structure in the spectral variation of transmission and absorption of solar radiation in vegetation canopies. *IEEE Trans. Geosci. Remote Sens.*, **39,** 241–253.

Pinty, B., and Coauthors, 2001: Radiation Transfer Model Intercomparison (RAMI) exercise. *J. Geophys. Res.*, **106,** 11 937–11 956.

——, and Coauthors, 2004: Radiation Transfer Model Intercomparison (RAMI) exercise: Results from the second phase. *J. Geophys. Res.*, **109,** D06210, doi:10.1029/2003JD004252.

Ricchiazzi, P., S. R. Yang, C. Gautier, and D. Sowle, 1998: SBDART: A research and teaching software tool for plane-parallel radiative transfer in the earth's atmosphere. *Bull. Amer. Meteor. Soc.*, **79,** 2101–2114.

Ross, J., 1981: *The Radiation Regime and Architecture of Plant Stands*. Springer, 420 pp.

Schull, M. A., and Coauthors, 2007: Physical interpretation of the correlation between multi-angle spectral data and canopy height. *Geophys. Res. Lett.*, **34,** L18405, doi:10.1029/2007GL031143.

——, and Coauthors, 2011: Canopy spectral invariants. Part 2: Application to classification of forest types from hyperspectral data. *J. Quant. Spectrosc. Radiat. Transf.*, **112,** 736–750.

Slingo, A., 1989: A GCM parameterization for the shortwave radiative properties of water clouds. *J. Atmos. Sci.*, **46,** 1419–1427.

Smolander, S., and P. Stenberg, 2005: Simple parameterizations of the radiation budget of uniform broadleaved and coniferous canopies. *Remote Sens. Environ.*, **94,** 355–363.

Stamnes, K., S.-C. Tsay, W. J. Wiscombe, and K. Jayaweera, 1988: Numerically stable algorithm for discrete-ordinate-method radiative transfer in multiple scattering and emitting layered media. *Appl. Opt.*, **27,** 2502–2509.

Twomey, S., and C. F. Bohren, 1980: Simple approximations for calculations of absorption in clouds. *J. Atmos. Sci.*, **37,** 2086–2094.

Vladimirov, V. S., 1963: *Mathematical Problems in the One-Velocity Theory of Particle Transport.* Vol. AECL-1661, Atomic Energy of Canada Ltd., 302 pp.

Wang, Y. J., and Coauthors, 2003: A new parameterization of canopy spectral response to incident solar radiation: Case study with hyperspectral data from pine dominant forest. *Remote Sens. Environ.*, **85,** 304–315.